Inorganic Chemistry

ARTICLE

pubs.acs.org/IC

Reversible Capture of Small Molecules On Bimetallaborane Clusters: Synthesis, Structural Characterization, and Photophysical Aspects

Jonathan Bould,*[,†,⊥] Tomáš Baše,[†] Michael G. S. Londesborough,[†] Luis A. Oro,[‡] Ramón Macías,[‡] John D. Kennedy,[⊥] Pavel Kubát,[§] Marcel Fuciman,[∥] Tomáš Polívka,[∥] and Kamil Lang*[,†]

[†]Institute of Inorganic Chemistry, Academy of Sciences of the Czech Republic, v.v.i., 250 68 Husinec-Řež, Czech Republic

[‡]Instituto Universitario de Catálisis Homogénea, Universidad de Zaragoza, 50009-Zaragoza, Spain

[§]J. Heyrovský Institute of Physical Chemistry, Academy of Sciences of the Czech Republic, v.v.i., Dolejškova 3, 182 23 Prague 8, Czech Republic

[∥]Institute of Physical Biology, University of South Bohemia, Zámek 136, 373 33 Nové Hrady, Czech Republic

[⊥]The School of Chemistry of the University of Leeds, Leeds LS2 9JT, U.K.

Supporting Information

ABSTRACT: Metallaborane compounds containing two adjacent metal atoms, $[(PMe_2Ph)_4MM'B_{10}H_{10}]$ (where MM′ = Pt_2, **1**; PtPd, **7**; Pd_2, **8**), have been synthesized, and their propensity to sequester O_2, CO, and SO_2 and to then release them under pulsed and continuous irradiation are described. Only $[(PMe_2Ph)_4Pt_2B_{10}H_{10}]$, **1**, undergoes reversible binding of O_2 to form $[(PMe_2Ph)_4(O_2)Pt_2B_{10}H_{10}]$ **3**, but solutions of **1**, **7**, and **8** all quantitatively take up CO across their metal−metal vectors to form $[(PMe_2Ph)_4(CO)Pt_2B_{10}H_{10}]$ **4**, $[(PMe_2Ph)_4(CO)PtPdB_{10}H_{10}]$ **10**, and $[(PMe_2Ph)_4(CO)Pd_2B_{10}H_{10}]$ **11**, respectively. Crystallographically determined interatomic M−M distances and infrared CO stretching frequencies show that the CO molecule is bound progressively more weakly in the sequence {PtPt} > {PtPd} > {PdPd}. Similarly, SO_2 forms $[(PMe_2Ph)_4(SO_2)Pt_2B_{10}H_{10}]$ **5**, $[(PMe_2Ph)_4(SO_2)PtPdB_{10}H_{10}]$ **12**, and $[(PMe_2Ph)_4(SO_2)Pd_2B_{10}H_{10}]$ **13** with progressively weaker binding of the SO_2 molecule. The uptake and release of gas molecules are accompanied by changes in their absorption spectra. Nanosecond transient absorption spectroscopy clearly shows that the O_2 and CO molecules are liberated from the bimetallic binding site with high quantum yields of about 0.6. For **3**, in addition to dioxygen release in the triplet ground state, singlet oxygen $O_2(^1\Delta_g)$ was also detected with a quantum yield <0.01. In most cases, the release and rebinding of the gas molecules can be cycled with little photodegradation of the compounds. Femtosecond transient absorption spectroscopy further reveals that the photorelease of the O_2 and CO molecules, from **3** and **4** respectively, is an ultrafast process taking place on a time scale of tens of picoseconds. For SO_2, the release is even faster (<1 ps), but only in the case of mixed metal PtPd adducts, most probably because of the metal−metal bonding asymmetry in the mixed metal clusters; for the corresponding symmetric Pt_2 and Pd_2 adducts, **5** and **13**, the release of SO_2 is significantly slower (>1 ns). All these compounds may have potential to serve as light-triggered local and instantaneous sources of the studied gases.

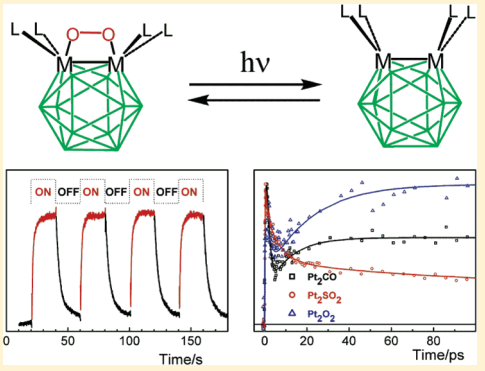

INTRODUCTION

The reversible binding of small molecules on metal atoms, metal−metal vectors, and metal surfaces is often used, both in Nature and in industry, to overcome otherwise insurmountable thermodynamic barriers in chemistry. Examples of uses found for this type of interaction are numerous and perhaps the most important one is the reversible uptake of dioxygen on the iron center in hemoglobin. In this context, we have previously reported the quantitative and reversible uptake of O_2 by the metal−metal linkage in the intensely dark purple icosahedral twelve-vertex bimetallaborane cluster compound $[(PMe_2Ph)_4Pt_2B_{10}H_{10}]$ **1** made from the reaction of $[PtCl_2(PMe_2Ph)_2]$ with $[(PMe_2Ph)_2PtB_{10}H_{12}]$ **2** to give the yellow-orange dioxygen bimetallaborane complex $[(PMe_2Ph)_4(O_2)Pt_2B_{10}H_{10}]$ **3** (Scheme 1).[1] The reversibility is readily induced by pressure reduction or by mild warming. Also, by analogy with the competitive binding of gases other than oxygen to hemoglobin, compound **1** interacts with CO and SO_2 to give tan-colored $[(PMe_2Ph)_4(CO)Pt_2B_{10}H_{10}]$ **4** and orange $[(PMe_2Ph)_4(SO_2)Pt_2B_{10}H_{10}]$ **5** (Scheme 1).[1b] In a similar manner to O_2, the uptake of CO and SO_2 by **1** occurs very readily and quantitatively, but in these cases the additions are not reversible under normal conditions of pressure reduction or mild heating. Reversible SO_2

Received: February 22, 2011
Published: July 21, 2011

Scheme 1. Schematic Structures of Investigated Compounds Showing Compound Numbering and Acronyms Used in the Text

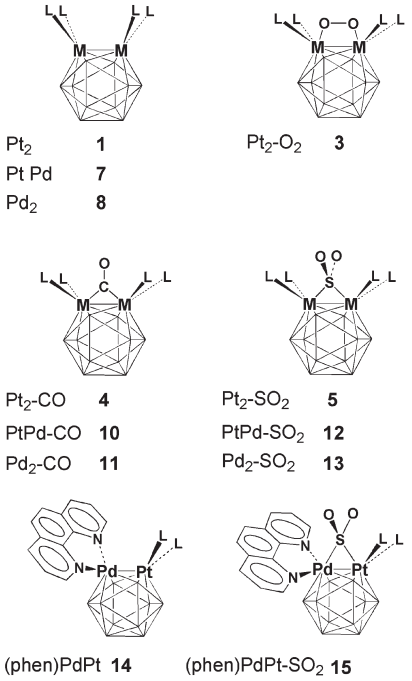

and/or CO uptake on monometallic[2] or bimetallic species[3−6] has been reported previously, but rarely in conjunction with oxygen uptake[7] as occurs in the system we describe here. The reversibility of O_2 addition to **1** to give **3** contrasts with the irreversible formation of the only other known analogous O_2 complex to a metal−metal-bonded system, that is, the formation of dark purple $[Ir_2I_2(CO)_2(O_2)(Ph_2PCH_2PPh_2)_2]$ **6** from $[Ir_2I_2(CO)_2(Ph_2PCH_2PPh_2)_2]$, first reported 20 years ago.[8]

In this paper, we investigate whether the sequestration of SO_2 and CO by our bimetallic system can be made to be reversible by changing one or both of the metal atoms from platinum to palladium. Additionally, we demonstrate that sequestered molecules of O_2, CO, and SO_2 can be reversibly ejected by pulsed UV−vis irradiation: here, time-resolved spectroscopic studies spanning the time-range from femtoseconds to microseconds provide a quantitative refinement of the qualitative observations obtained from steady-state UV−vis spectroscopy.

As an easy reference, and as an aid to the reader, Scheme 1 shows a schematic listing of the structures described in this paper and their compound numbers. For example, $[(PMe_2Ph)_4(O_2)Pt_2B_{10}H_{10}]$ **3**, is referred to below as Pt_2-O_2 **3**.

RESULTS AND DISCUSSION

Compound Syntheses. The bimetallic compounds $[(PMe_2Ph)_4MM'B_{10}H_{10}]$ are synthesized by the addition of 2 equivalents of $KHBEt_3$ to suspensions of $[(PMe_2Ph)_2MB_{10}H_{12}]$ (M = Pt or Pd) in toluene at low temperature, followed by the addition of $[M'Cl_2(PMe_2Ph)_2]$ (MM′ = PtPt for **1**, PtPd for **7**, and PdPd for **8**) and slow warming to room temperature. The air-stable Pt_2 **1** and Pd_2 **8** compounds are then obtained essentially pure

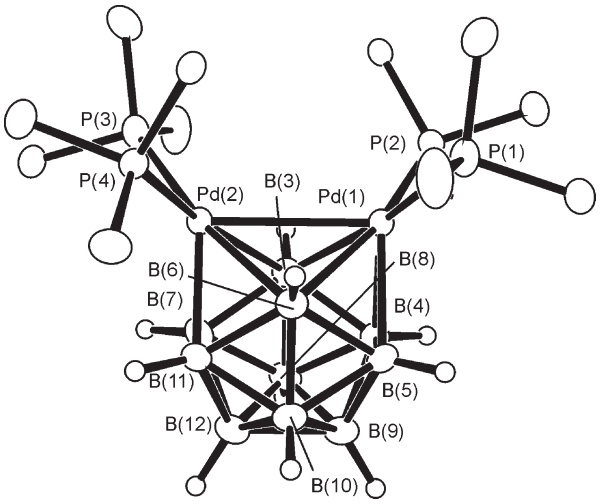

Figure 1. Representation of the crystallographically obtained molecular structure of $[(PMe_2Ph)_4Pd_2B_{10}H_{10}]$, Pd_2 **8**, showing the cluster numbering system employed, with 50% thermal ellipsoids for non-hydrogen atoms. The phenyl rings (except for the *ipso* carbon atoms) and methyl group hydrogen atoms are omitted to aid clarity. The molecule possesses a C_2 axis such that equivalent cluster positions are Pd(1)≡Pd(2), B(3)≡B(6), B(4)≡B(11), B(5)≡B(7), B(8)≡B(10), and B(9)≡B(12). Selected measured geometric parameters for Pd_2 **8** are listed in Table 1.

by filtration in yields of up to 76% and 57%, respectively, with the latter, new compound, affording a satisfactory elemental analysis. The yield for **1** is an improvement on the 23% previously reported from preparations using tetrahydrofuran (THF) as solvent.[1b] Interestingly, it may also be noted that a crystalline precipitate of the Pt_2 **1** compound may also be obtained in about 50% yield from a toluene solution of $[(PMe_2Ph)_2PtB_{10}H_{12}]$ at reflux containing added PMe_2Ph[9] (see Experimental Section). Single-crystal X-ray diffraction data were obtained for the dipalladium compound **8** (Figure 1), together with the cluster numbering scheme. The molecular structure of Pt_2 **1** is previously reported.[1] The isolation of the mixed palladium−platinum analogue PtPd **7** from the reaction mixture using $KHBEt_3$ is less straightforward. Crystallization of the purple-brown solid afforded in the reaction is difficult and results in some decomposition of the compound. Nevertheless, sufficient quantities for a satisfactory elemental analysis and for further reaction chemistry have been obtained (31% yield). Its identity is also readily inferred from the results of multinuclear NMR spectroscopy in comparison with those for the Pt_2 **1** and Pd_2 **8**, (Supporting Information) and from its well-characterized adducts with SO_2 and CO, which were made in situ as described below.

The diplatinum compound **1** was first isolated in 1985,[9] though its propensity to take up O_2 was not recognized until some 20 years later.[1a] The dark-purple crystalline solid exhibits excellent air stability; a small sample of the compound, stored in a sample tube with plastic cap, was found to be unchanged after 20 years. The two new species PtPd **7** and Pd_2 **8** are also air-stable in the solid state, but samples of Pd_2 **8** have been observed to degrade over a period of a few months. They are, however, stable in chlorinated solvents in the absence of air. In the presence of air, solutions of Pd_2 **8** in $CHCl_3$ are not stable, perhaps suggesting activation of atmospheric oxygen via a transient weak dioxygen

dx.doi.org/10.1021/ic200374k |*Inorg. Chem.* 2011, 50, 7511–7523

Table 1. Selected Measured Interatomic Dimensions from Single-Crystal X-ray Diffraction Studies with Selected Equivalent DFT Calculated Dimensions in [Square Brackets]

	Pt_2	Pd_2	Pt_2-CO	PtPd-CO	Pd_2-CO	Pt_2-SO_2	PtPd-SO_2	Pd_2-SO_2
	1[a,c]	**8**[c]	**4**[a]	**10**[b]	**11**	**5**[a]	**12**[b]	**13**
M(1)−M(2)	2.9552(4)	2.9163(3)	2.7487(3)	2.749(3)	2.7491(6)	2.8194(4)	2.810(7)	2.8041(6)
	[2.9545]	[2.9095]	[2.8246]	[2.7961]	[2.785]	[2.8728]	[2.8545]	[2.8375]
M(1)−P(1)	2.3344(4)	2.3860(6)	2.3402(16)	2.3416(18)	2.4007(11)	2.383(3)	2.384(4)	2.4172(13)
M(1)−P(2)	2.3382(4)	2.3806(6)	2.3516(17)	2.3656(17)	2.4013(9)	2.353(3)	2.351(4)	2.3798(13)
M(2)−P(3)			2.3331(17)	2.378(3)	2.4090(12)	2.345(2)	2.421(6)	2.4276(15)
M(2)−P(4)			2.3440(17)	2.419(4)	2.4006(8)	2.376(2)	2.379(7)	2.3915(13)
M(1)−C/S			2.098(6)	2.112(4)	2.148(3)	2.388(2)	2.367(4)	2.3689(13)
			[2.219]	[2.260]	[2.249]	[2.5942]	[2.6465]	[2.5909]
M(2)−C/S			2.106(6)	2.167(5)	2.175(3)	2.355(2)	2.405(7)	2.4139(13)
			[2.219]	[2.203]	[2.249]	[2.5942]	[2.5592]	[2.5909]
M(1)−B(3)	2.3626(17)	2.346(3)	2.332(7)	2.314(4)	2.329(3)	2.339(10)	2.284(10)	2.304(5)
M(1)−B(4)	2.2035(18)	2.212(3)	2.264(7)	2.268(4)	2.293(3)	2.258(10)	2.232(9)	2.260(5)
M(1)−B(5)	2.2225(18)	2.233(3)	2.255(7)	2.265(4)	2.280(3)	2.219(12)	2.239(9)	2.253(5)
M(1)−B(6)			2.305(6)	2.333(4)	2.305(3)	2.322(10)	2.328(10)	2.313(5)
M(2)−B(3)			2.298(7)	2.325(5)	2.306(3)	2.301(9)	2.330(11)	2.304(5)
M(2)−B(6)			2.348(7)	2.291(5)	2.344(3)	2.348(6)	2.329(11)	2.324(5)
M(2)−B(7)			2.280(6)	2.261(5)	2.269(3)	2.258(10)	2.223(11)	2.237(5)
M(2)−B(11)			2.266(6)	2.268(5)	2.284(3)	2.219(12)	2.229(12)	2.262(6)
S(1)\C(1)−O(1)			1.174(7)	1.153(4)	1.158(3)	1.454(7)	1.458(6)	1.455(4)
			[1.1676]	[1.1623]	[1.1581]	[1.490]	[1.486]	[1.485]
S(1)−O(2)						1.461(7)	1.456(6)	1.460(4)
O(1)−S(1)−O(2)						113.7(4)	112.7(4)	113.5(2)
						[115.7]	[115.8]	[116.1]
M(1)−C(1)\S(1)−M(2)			81.36(19)	79.94(15)	78.97(10)	72.94(6)	72.14(18)	71.78(4)
			[79.1]	[77.6]	[76.5]	[67.2]	[66.5]	[66.4]

[a] Data from reference 1b. [b] M(1) = Pt. [c] There is crystallographically imposed 2-fold symmetry for compounds **1** and **8**, such that M(1), P(1), P(2), B(3), B(4), and B(5) are equivalent to M(2), P(3), P(4), B(6), B(11), and B(7), respectively.

adduct, although monitoring by ^{11}B NMR spectroscopy shows no sign of such an intermediate. We have not yet conducted a detailed investigation of the products from these air-induced reactivities, but we have established by a single-crystal X-ray diffractions analysis that one product is a yellow-colored compound $[(Cl)(PMe_2Ph)_3Pd_2B_{10}H_9(PMe_2Ph)]$ **9** (Figure S1, Supporting Information). Here, a PMe_2Ph ligand has been displaced from a palladium center by a chlorine substituent, and the PMe_2Ph has moved onto a boron atom. This results in a more open crevice for access to the dipalladium center, which augurs for some synthetic usefulness for this type of process, as fine tailoring of these dimetal species for small-molecule sequestration and activation will involve both entropic adjustment of the cavity size about the dimetal center and also electronic adjustment by substituents on the boron atoms of the cluster. The diplatinum analogue of **9** was isolated in the original work that resulted in the Pt_2 **1** compound.[9]

Structural Studies of the CO and SO_2 Complexes. We initially assessed the system by DFT calculation of molecular geometry at the B3LYP/6-31G*/LANL2DZ level[10] to build up a matrix of information as to how modification of the metal would be expected to weaken or strengthen the binding of the small molecules, to validate our experimental observations thus enabling us to identify future synthetic targets. Details on these preliminary predictive calculations may be seen in the Supporting Information but, for comparison purposes, selected calculated geometric dimensions for the molecules reported here are listed

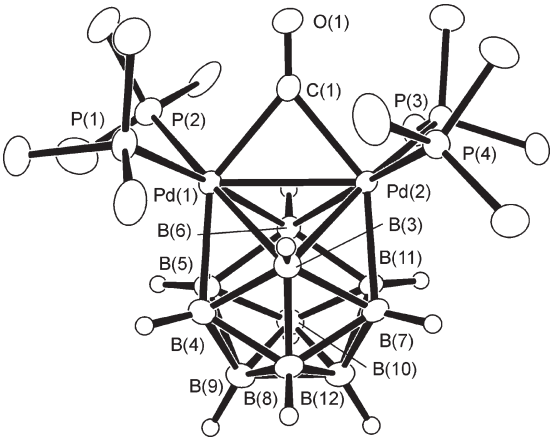

Figure 2. Representation of the crystallographically determined molecular structure of $[(PMe_2Ph)_4(CO)Pd_2B_{10}H_{10}]$, Pd_2-CO **11**, displayed with 50% thermal ellipsoids for non-hydrogen atoms. Phenyl group atoms (with the exception of the *ipso* carbon atoms) and the methyl group hydrogen atoms are omitted to aid clarity. Selected measured geometric parameters are listed in Table 1.

dx.doi.org/10.1021/ic200374k |*Inorg. Chem.* 2011, 50, 7511–7523

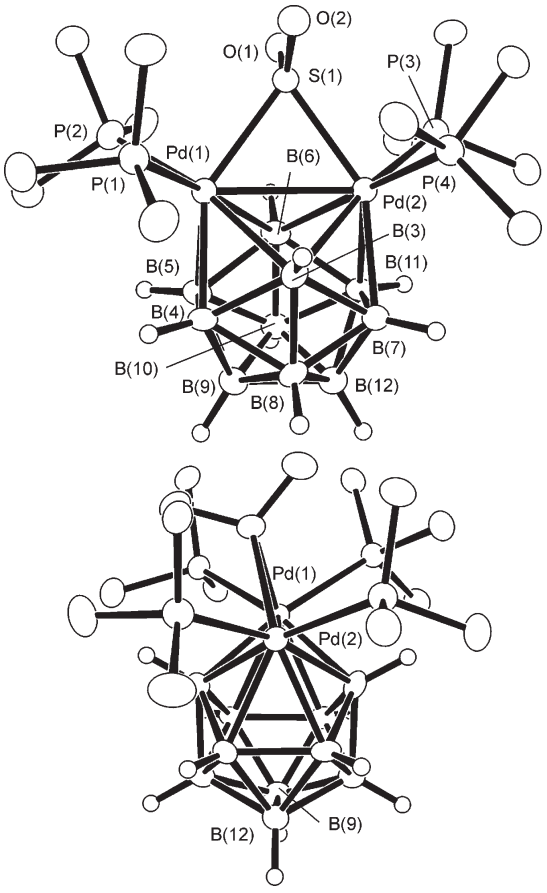

Figure 3. Representation of the crystallographically determined molecular structure of $[(PMe_2Ph)_4(SO_2)Pd_2B_{10}H_{10}]$, Pd_2-SO_2 **13**, displayed with 50% thermal ellipsoids for non-hydrogen atoms. Phenyl group atoms, with the exception of the *ipso* carbon atoms and the methyl group hydrogen atoms are omitted to aid clarity. The lower diagram shows a side view illustrating the tilting of the SO_2 group with respect to the Pd(1)Pd(2)B(9)B(12) plane. The corresponding representation of the molecular structure of the PtPd-SO_2 **12** analogue is visually isostructural and is therefore not shown. Selected measured geometric parameters for **12** and **13** are listed in Table 1.

in Table 1 and pertinent values shown in the Supporting Information are referred to in the text as required.

In contrast to Pt_2 **1**, no color changes are observed when dichloromethane solutions of PtPd **7** or Pd_2 **8** are saturated with dioxygen, and NMR spectroscopy shows no change. This reflects the trend in the calculated O−O interatomic distances that feature a shortening from 1.367 Å for Pt_2-O_2 to 1.351 Å for PtPd-O_2 to 1.336 Å for Pd_2-O_2 (Scheme S4, Supporting Information), synonymous with a weakening the interaction between dioxygen and the metal−metal cluster vector.

Under one atmosphere pressure of CO at room temperature, solutions of PtPd **7** and Pd_2 **8** exhibit immediate color changes from brown and dark purple-red respectively, to a pale tan-yellow in both cases. IR spectroscopy indicates the formation a CO adduct [ν(CO) 1847 cm^{-1} for PtPd-CO **10**, 1882 cm^{-1} for Pd_2-CO **11** (Pt_2-CO **4** is 1810 cm^{-1})[1b]]. This was confirmed by a single-crystal X-ray diffraction studies on **10** and **11** (Figure 2) and by ^{1}H, ^{11}B, and ^{31}P NMR spectroscopy which show that the addition is quantitative. Selected calculated and experimental geometric parameters together with those of the Pt_2-CO **4**

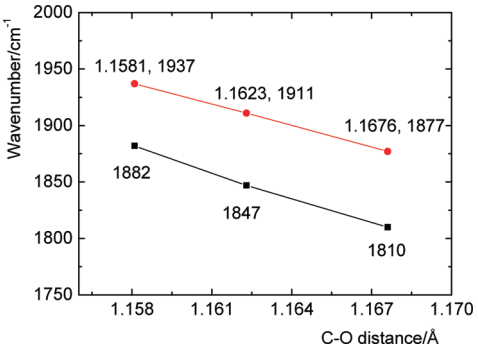

Figure 4. Measured (lower line) and DFT-calculated (upper line) infrared stretching frequencies of the CO group in Pt_2-CO **4** (right) PtPd-CO **10** (center) and Pd_2-CO **11** (left), plotted against the B3LYP/6-31G*/LANL2DZ calculated C−O distance.

analogue are listed in Table 1. The overall structure of PtPd-CO **10** is very similar to that for Pd_2-CO **11**, but the disordered positions for the Pt and Pd atoms and for two of the PMe_2Ph groups means that the measured interatomic dimensions are less precise than those for the Pt_2-CO **4** and Pd_2-CO **11**, thus precluding a detailed comparison.

Sulfur dioxide reacts with PtPd **7** and Pd_2 **8** by addition to the metal−metal vector to give the two yellow-orange colored species PtPd-SO_2 **12** and Pd_2-SO_2 **13**, respectively. The reaction is also immediate and quantitative, as with Pt_2 **1**, which gives light orange Pt_2-SO_2 **5**.[1b] The compounds PtPd-SO_2 **12** and Pd_2-SO_2 **13** are characterized by single-crystal X-ray diffraction analyses (Figure 3, Table 1) and by NMR spectroscopy (Experimental Section; a detailed analysis of the ^{11}B NMR spectra of the new compounds described in this paper may be also found in the Supporting Information).

All three SO_2 adducts, Pt_2-SO_2 **5**, PtPd-SO_2 **12**, and Pd_2-SO_2 **13**, exhibit qualitatively very similar SO_2 binding modes to the metal−metal unit. The sulfur atoms bridge the metal−metal linkage, which is not cleaved, and the sulfur atom exhibits approximately tetrahedral coordination to the two metal atoms and to the two oxygen atoms. In quantitative terms, with allowance for the disorder in the crystallographic structure of PtPd-SO_2 **12**, the density functional theory (DFT) predictions are nicely supported (Table 1), showing progressive lengthening of the metal-to-sulfur distances and progressively decreasing differences for the intermetal separations, from 2.8194(4) [2.8728 calc.] for **5**, to 2.8041(6) [2.8375 calc.] Å for **13**. Some minor differences are evident between the experimentally determined structure and the calculated structure, such as a tilting of the SO_2 group with respect to the plane defined by Pd(1)Pd(2)B(9)B(12), which is not evident in the calculated structure. This may reasonably be ascribed to the effect of the packing of the SO_2 molecule within the PMe_2Ph ligand sphere, which is itself constrained by crystal packing forces. The organyl groups were replaced by H atoms to reduce computation time and thus the effect due to the constraints of the organyl groups would not be seen.

The calculated intermetal distances are longer than the measured ones by up to about 0.05 Å but this is not unexpected for third-row transition elements,[11] and other distances match more closely. The trends are well reproduced, and in particular there is a prediction of progressive weakening to the level of reversibility: the duly observed reversibilities of the additions of

dx.doi.org/10.1021/ic200374k |*Inorg. Chem.* 2011, 50, 7511–7523

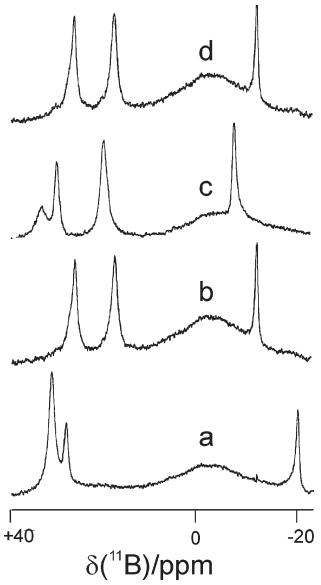

Figure 5. ^{11}B-{^{1}H(broadband)} NMR spectra of aliquots of a single solution of Pd_2 **8** in CD_2Cl_2/CH_2Cl_2 before (trace a) and after (trace b) addition of CO to give Pd_2-CO **11**. Addition of SO_2 to (b) quantitatively affords Pd_2-SO_2 **13** (trace c), but bubbling CO through the warmed solution of **13** displaces the SO_2 to reform Pd_2-CO **11**, (trace d). The large "hump" in the spectra centered at $\delta(^{11}B)$ about −5 ppm is due to boron in the Pyrex NMR sample tube.

CO and SO_2 to the PtPd **7** and Pd_2 **8** compounds are described and discussed below.

Thus, for the CO adducts, the calculated and measured C−O distances are equal within experimental uncertainties, namely, 1.174(7) [1.168] in Pt_2-CO **4**, 1.153(4) [1.162] in PtPd-CO **10** (NB: a considerable disorder in the single-crystal used in the X-ray study renders this measured value less reliable), and 1.158(3) [1.158] in Pd_2-CO **11**. Plots of the calculated metal separations versus the measured and calculated infrared stretching frequencies show a linear progression (Figure 4). Although there is a systematic overestimation of the stretching frequency of about 60 cm^{-1}, this mirrors the systematic errors in the distances to the metals, and is consistent along the series.

In contrast to the diplatinum system, the addition of CO to Pd_2 **8** is readily reversible, and removal of the solvent from solutions of Pd_2-CO **11** on a rotary evaporator results in the loss of the CO to reform Pd_2 **8**. CO may also be displaced by addition of SO_2 to form Pd_2-SO_2 **13**, but the SO_2 is also not strongly bound, and it may in turn be replaced by bubbling CO through solutions of Pd_2-SO_2 **13** in warm dichloromethane, as illustrated in Figure 5. The sulfur dioxide unit may be similarly displaced by CO from the mixed-metal adduct PtPd-SO_2 **12**, although it requires an extended time at the reflux temperature of CH_2Cl_2 to accomplish this. This reluctance is in line with the slightly stronger binding to the PtPd vector suggested by the calculated and measured intramolecular dimensions. In solution these compounds probably form an equilibrium mixture involving the complexed and uncomplexed metallaborane which is driven fully to product by the presence of excess CO or SO_2. A more direct example showing presence of such an equilibrium is in the SO_2 adduct of [(phenanthroline)Pd(PMe_2Ph)$_2$Pt$B_{10}H_{10}$], (phen)PdPt **14**, namely, [(phenanthroline)Pd(PMe_2Ph)$_2$Pt-(SO_2)$B_{10}H_{10}$], (phen)PdPt-SO_2 **15**. Here, the ^{11}B spectrum of

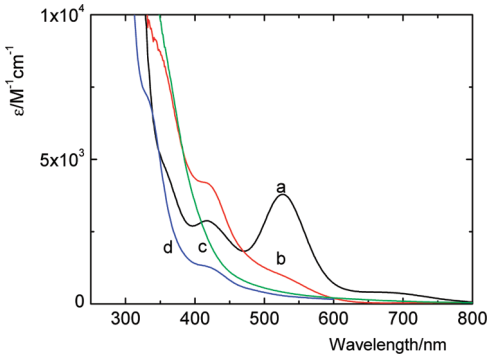

Figure 6. Absorption spectra in CH_2Cl_2 of Pt_2 **1** (a) and corresponding adducts Pt_2-O_2 **3** (b), Pt_2-SO_2 **5** (c), and Pt_2-CO **4** (d).

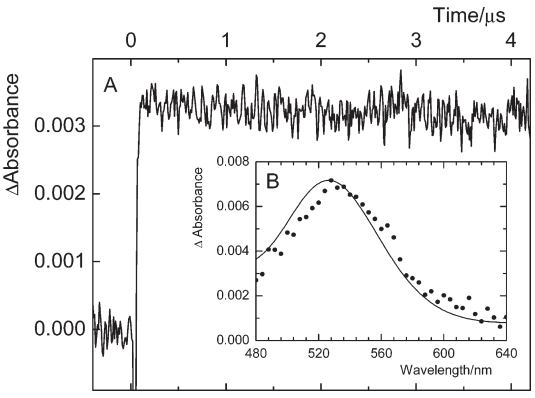

Figure 7. (A) Photorelease of CO after excitation of Pt_2-CO **4** (ca. 100 μM in CH_2Cl_2) by a 425 nm laser pulse (ca. 2 mJ/pulse), measured at 524 nm. (B) Inset: transient absorption spectrum recorded 1 μs after excitation by a 308 nm laser pulse (ca. 15 mJ/pulse) compared with the normalized absorption spectrum of Pt_2 **1** (solid line) in CH_2Cl_2.

crystalline samples of (phen)PdPt-SO_2 **15** dissolved in CD_2Cl_2 shows that it forms an equilibrium mixture of **14** and **15** which requires the addition of excess SO_2 to push it to pure solutions of **15**.[12]

That O_2, CO, and SO_2 are released by the displacement or by warming solutions differently according to the identity of the metals, indicates that the reversibility of the binding is a tunable feature which might be of interest for, inter alia, the design of sensor materials and as handy sources of gas fluxes in a defined environment. For many possible applications, an external trigger to engender the instant release of the bound molecule would be required. This led us to examine the photophysical properties of the adducts, as photolysis by laser pulses using specific wavelengths could be a suitable and well-defined trigger for such a process.

Absorption Spectra. Figure 6 shows absorption spectra of Pt_2 **1** and its O_2, CO, and SO_2 adducts. Compound Pt_2 **1** exhibits a quite distinctive absorption band at 527 nm, which is well separated from other electronic transitions. Reaction of Pt_2 **1** with O_2, CO, or SO_2 is instantaneous, and the adduct formation is accompanied by the disappearance of this absorption band. In the case of Pt_2-SO_2 **5**, absorption below 350 nm is obscured by that of free SO_2 (Figure S2c, Supporting Information). We have included (phen)PdPt **14** and (phen)PdPt-SO_2 **15**[12] to provide extra examples of the mixed metal species. The absorption

dx.doi.org/10.1021/ic200374k |*Inorg. Chem.* 2011, 50, 7511–7523

changes observed for PtPd **7** and (phen)PdPt **14** are comparable to those in Pt_2 **1**, with the respective absorption bands at 495 and 528 nm disappearing after the addition of SO_2 (Figures S3, Supporting Information). Large absorption changes are also observed after the formation of Pd_2-SO_2 **13** from Pd_2 **8** (Figure S2, Supporting Information). In all cases, the adducts have sufficiently different absorption spectra when compared with the original cluster compounds to allow the spectroscopic monitoring of the reactions occurring in solution.

Nanosecond Laser Flash Photolysis. Nanosecond transient absorption spectroscopy of the Pt_2-CO **4** adduct shows the absorption changes (Figure 7) that arise from the liberation of CO from the bimetallic binding site. The changes occur within an excitation pulse width (ca. 28 ns) (Figure 7A), and the transient absorption spectrum nicely matches the absorption spectrum of Pt_2 **1** (Figure 7B), confirming that the photoproduct is indeed Pt_2 **1**. Furthermore, it is apparent that CO molecules are liberated from the bimetallic binding site very quickly. The diffusion-controlled back-reaction proceeds on a millisecond time scale (Figure S4, Supporting Information) that depends on the concentration of dissolved CO.

The quantum yield of the CO release, measured to be 0.60 ± 0.03 upon 308 nm irradiation, shows a high efficiency of scission of the Pt_2-CO linkage. To the best of our knowledge, the thermodynamics and the mechanism of CO photorelease and rebinding have mostly been studied with heme model compounds to understand processes through which heme proteins perform their physiological function.[13] However, these processes are complex because of a heme center spin transition and, in some cases, because of the formation of a four-coordinate heme center or other factors, such as the flexing shape of the protein crevice, and cannot therefore be compared to the behavior of the Pt_2-CO **4** adduct.

The results further show that Pt_2-SO_2 **5** behaves similarly to Pt_2-CO **4** even though the absorption changes are smaller (data not shown). Because of the absorption of dissolved SO_2 below 350 nm, the quantum yield of the SO_2 photorelease from Pt_2-SO_2 **5** could not be measured. The adducts Pd_2-SO_2 **13**, PtPd-SO_2 **12**, and (phen)PdPt-SO_2 **15** also instantly release SO_2 (Figure S5, Supporting Information), and the liberated SO_2 recombines with the corresponding cluster to give the original adducts. There is little information in the literature on the reversible binding of SO_2 to metal complexes. For example, although it has previously been shown that some four-coordinate iridium species such as Vaska's compound $[IrCl(CO)(PPh_3)_2]$,[2b] and platinum compounds containing the terdentate-coordinating monoanionic $[2,6\text{-}(CH_2NMe_2)_2\text{-}C_6H_3]^-$ ligand,[3b,14] can reversibly bind SO_2, there are no reports, to our knowledge, on the release of SO_2 upon UV−vis irradiation.

Of the bimetallic boron clusters reported here, only Pt_2 **1** binds dioxygen.[1b] Like Pt_2-CO **4**, the photorelease of O_2 from Pt_2-O_2 **3** occurs with a high quantum yield of 0.58 ± 0.03 after excitation by a 308 nm pulse. In addition to dioxygen in the ground triplet state [i.e., $O_2(^3\Sigma_g^-)$], a contribution of singlet oxygen $O_2(^1\Delta_g)$, was detected. This is surprising, as $O_2(^1\Delta_g)$ is most often produced by energy transfer to the dioxygen ground state from an electronically excited triplet state of a photosensitizer molecule.[15] Under our conditions, we can exclude the photosensitized formation of $O_2(^1\Delta_g)$ as no long-lived excited states were detected (see below). Thus, the $O_2(^1\Delta_g)$ formation is clearly a result of the relaxation of excited states of the dioxygen adduct. To assess the efficiency of the $O_2(^1\Delta_g)$ generation we have measured its photoluminescence at 1270 nm (Figure S6, Supporting Information), as emission at this wavelength arises from relaxation of $O_2(^1\Delta_g)$ back to the triplet ground state $O_2(^3\Sigma_g^-)$. The quantum yield of $O_2(^1\Delta_g)$ formation, Φ_Δ, estimated using a porphyrin standard,[16] is below 0.01, thus indicating that the splitting channel leading to $O_2(^1\Delta_g)$ is of minor importance, although the option of modifying the system specifically to generate $^1\Delta_g$ dioxygen is a future possibility that we are currently pursuing. Following photorelease, the bare diplatinum unit Pt_2 **1** rebinds O_2, albeit with some minor photodegradation being evident. Indeed, the lifetime of $O_2(^1\Delta_g)$, which is a measure of its reactivity with dissolved molecules, is dictated by the quenching efficiency of the metallaborane unit (Figure S6, Supporting Information). As a result, the measured lifetime for $O_2(^1\Delta_g)$ of 45 to 55 μs is much less that the reported value of 100 μs in pure CH_2Cl_2 in the absence of any singlet oxygen quenching activity.[16]

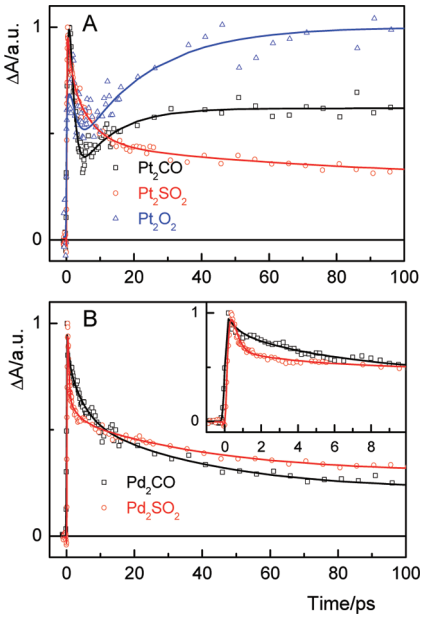

Figure 8. Kinetics following about 130 fs UV-excitation of the O_2, CO, and SO_2 adducts of (A) Pt_2 **1** and (B) Pd_2 **8** saturated with the added respective gases. Excitation is at 395 nm, with a probing wavelength of 535 nm for Pt_2-O_2 **3**, Pt-CO **4**, and Pt_2-SO_2 **5**, and of 540 nm for Pd_2-CO **11** and Pd_2-SO_2 **13**. All kinetics are normalized to maxima, with the solid lines corresponding to fits obtained from global fitting.

For comparison purposes, it may be noted that some binuclear μ-superoxo- and μ -peroxo cobalt complexes similarly produce ground-state dioxygen upon irradiation.[17] Some mono-nuclear complexes also eliminate triplet-state dioxygen. For example, $[IrCl(O_2)(CO)(PPh_3)_2]$ does so with a quantum yield of up to 0.43 and, as with Pt_2-O_2 **3**, the quantum yield Φ_Δ is low at 0.03.[18] Conversely, the photolysis of the oxodiperoxomolybdenum(VI) complex, $[MoO(O_2)_2]$, produces $O_2(^1\Delta_g)$ with Φ_Δ up to 0.42 depending on the excitation wavelength.[19] The complex producing $O_2(^1\Delta_g)$ upon photolysis, with a behavior most similar to Pt_2-O_2 **3**, is the bis(triphenylphosphine)dioxygenplatinum peroxo complex $[(Ph_3P)_2Pt(O_2)]$; for this compound, this behavior is attributed to a ligand (i.e., O_2) transition with a ligand-to-metal ($O_2 \rightarrow Pt$) charge transfer contribution.[20] Unfortunately, no Φ_Δ values were given. To the best of our knowledge, Pt_2-O_2 **3**, is the *only* example of a

dx.doi.org/10.1021/ic200374k |*Inorg. Chem.* 2011, 50, 7511–7523

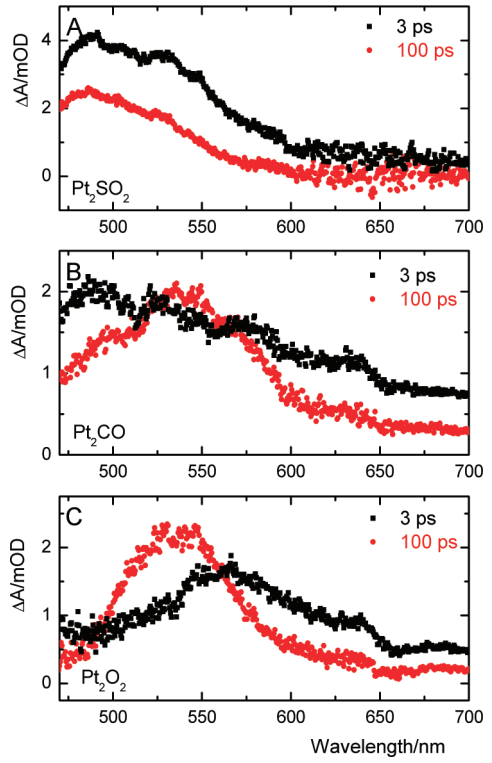

Figure 9. Transient absorption spectra of (A) Pt_2-SO_2 **5**, (B) Pt_2-CO **4**, and (C) Pt_2-O_2 **3** measured after two different delay intervals, 3 ps (black) and 100 ps (red), after excitation at 395 nm.

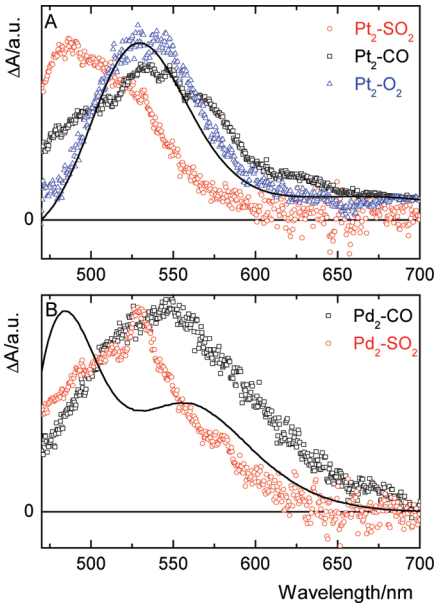

Figure 10. Transient absorption spectra of (A) Pt_2-SO_2 **5**, Pt_2-CO **4**, Pt_2-O_2 **3**, and (B) Pd_2-SO_2 **13**, Pd_2-CO **11** adducts recorded at 200 ps after excitation at 395 nm. Difference absorption spectra given as a difference between absorption spectra of the Pt_2 **1** and Pd_2 **8** clusters and the corresponding adducts are shown as solid lines for comparison.

bimetallic complex that reversibly binds dioxygen and releases it upon irradiation.

Femtosecond Transient Absorption. To obtain further insight into the photorelease mechanism of CO, SO_2, and O_2 molecules from the adducts following UV−vis irradiation, we studied the ultrafast dynamics upon excitation with pulses of about 130 fs duration centered at 395 nm. The resulting kinetics for the Pt_2- and Pd_2-based homometal adducts measured at 535 and 540 nm (the wavelengths where the photoproduced ground-state Pt_2 **1** and Pd_2 **8** compounds absorb) are shown in Figure 8. The kinetics of both of the compounds Pt_2-CO **4** and Pt_2-O_2 **3** reveal an initial fast decay followed by a rise component, whereas no corresponding rise component is observed for Pt_2-SO_2 **5**. To identify the origin of this qualitatively different behavior, we have compared the transient absorption spectra recorded after different delay intervals. While the transient absorption spectra of Pt_2-SO_2 **5** do not significantly differ in shape when recorded after delays of 3 and 100 ps, the broad and featureless spectra of Pt_2-O_2 **3** and Pt_2-CO **4** after 3 ps are replaced by a well-defined band centered at about 535 nm after a 100 ps delay (Figure 9). Further, a comparison of the transient absorption spectra at 200 ps with the difference absorption spectra (Figure 10) shows that, whereas the 200 ps spectra for Pt_2-O_2 **3** and Pt_2-CO **4** match well the absorption spectrum of Pt_2 **1** in the ground state, the transient absorption spectrum of Pt_2-SO_2 **5** peaks at 490 nm, and is thus significantly different from the 535 nm maximum.

The initial signals generated from Pt_2-CO **4** and Pt_2-O_2 **3** decay with a about 1.5 ps time constant. Since the transient absorption spectra at 3 ps do not contain bands attributable to the compound Pt_2 **1**, this decay can be assigned to a fast relaxation of the excited states of the corresponding adducts (Figure 9). The following rise, occurring with an 11 ps time constant in Pt_2-CO **4** and 20 ps in Pt_2-O_2 **3**, describes the formation of Pt_2 **1** in the ground state after the gas photorelease (Figures 9 and 10). In contrast, the excited-state relaxation of Pt_2-SO_2 **5** can be satisfactorily described by at least three decay components of 1, 6, and 80 ps. The photoproduct generated within the time window of the experiment is not ground-state Pt_2 **1** (Figure 10). Instead, an intermediate complex, which may be, for example, an excited Pt_2-SO_2 with one S−Pt bond broken, is formed within the first 200 ps, and the complete release of SO_2 from the Pt_2-SO_2 adduct probably takes place on a longer time scale inaccessible in our femtosecond experiments (>1 ns). This indicates that the binding affinity of SO_2 toward the Pt_2 **1** cluster is markedly greater than that of O_2 or CO, consistent with the conclusions from the results of DFT calculations (Supporting Information) and of experimental displacement reactions discussed in the section above.

For the dipalladium species, the kinetics recorded after the excitation of the Pd_2-based adducts shown in Figure 8 demonstrate a different binding to the Pd_2 **8** and Pt_2 **1** compounds for SO_2 compared to CO. Thus, the adduct Pd_2-SO_2 **13** behaves comparably to Pt_2-SO_2 **5** and the excited states decay multiexponentially with time constants of 0.3, 2.5, and 40 ps. This behavior demonstrates that the nature of the metal binding sites quantitatively affects the relaxation of the whole complex and that it is faster in Pt_2-SO_2 **5**. In contrast, however, the behavior of Pd_2-CO **11** qualitatively differs from that of Pt_2-CO **4**, as shown by the features of the transient spectra at 200 ps, which differ significantly from the difference absorption spectrum of Pd_2/Pd_2-CO (Figure 10). While excitation of Pt_2-CO **4** leads to the photorelease of CO with an 11 ps time constant, Pd_2-CO **11** undergoes excited-state relaxation with no formation of ground state Pd_2 **8** within the measured time window. For comparison here, it may be noted that the ultrafast kinetics of CO photorelease have been studied in

dx.doi.org/10.1021/ic200374k |*Inorg. Chem.* 2011, 50, 7511–7523

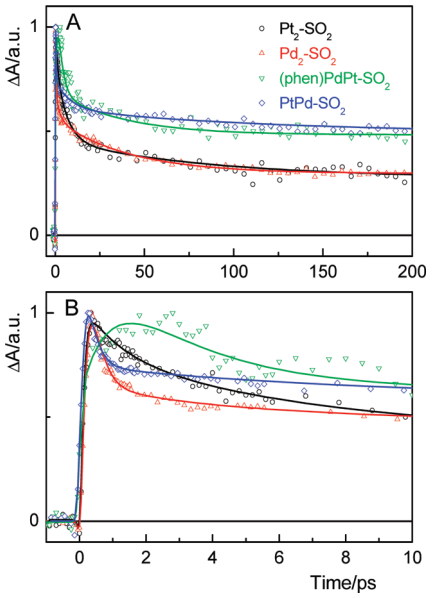

Figure 11. (A) Kinetics of the SO_2 complexes after excitation at 395 nm. Probing wavelengths were 530 nm for Pt_2-SO_2 **5**, 540 nm for Pd_2-SO_2 **13**, 520 nm for (phen)PdPt-SO_2 **15**, and 505 nm for PtPd-SO_2 **12**. The bottom panel (B) shows an expansion of the first 10 ps of the traces in the upper panel.

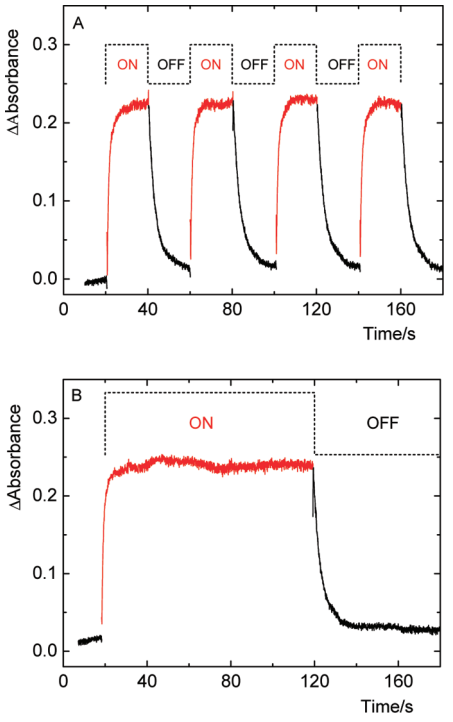

Figure 12. (A) Release and rebinding of O_2 under cyclic irradiation of Pt_2-O_2 **3** in CH_2Cl_2 (140 μM solution). The absorbance changes recorded at 524 nm during irradiation (light ON, red line) and dark periods (light OFF, black line), respectively, indicate the release of, and reverse binding of, O_2. The oxygen-saturated solution was irradiated by a Xe lamp (>370 nm). (B) Continuous irradiation for about 100 s under the same conditions as above.

detail in some heme compounds.[21,22] In these, the CO ligands are photodissociated instantaneously, and vibrational cooling of the ferrous ground state takes place in a few ps. Geminate recombination occurs from the nanosecond to millisecond time scales, and the CO molecules are stored within the protein matrix in docking sites.

Since both homometal SO_2 adducts Pt_2-SO_2 **5** and Pd_2-SO_2 **13** adducts have a comparable behavior, we also studied ultrafast dynamics of two SO_2-based adducts with mixed-metal binding sites, namely, PtPd-SO_2 **12** and (phen)PdPt-SO_2 **15** (Figure 11). The results clearly show that the nature of the metal atoms alters the amplitude and time constant of the initial fast component. In addition, the ultrafast dynamics are more complicated in (phen)PdPt-SO_2 **15**, showing a 0.8 ps rise that may be assigned to the formation of (phen)PdPt **14** because of the subpicosecond release of SO_2. This conclusion is also supported by a reasonable match between the transient absorption spectrum of (phen)-PdPt-SO_2 **15** taken at 200 ps and the corresponding difference absorption spectrum (Figure S7, Supporting Information). Thus, (phen)PdPt-SO_2 **15** may actually release the SO_2 molecule on a subpicosecond time scale, and the further dynamics, which are comparable to other SO_2-bound adducts, may then reflect a relaxation of (phen)PdPt **14** that is generated in a "hot" state. The time constants of this relaxation, as obtained from global fitting, are 2.5 and 35 ps. A similar situation occurs for PtPd-SO_2 **12**, for which the transient absorption spectrum recorded at 200 ps matches the PtPd/PtPd-SO_2 difference absorption spectrum (Figure S7, Supporting Information). However, no rise is detected; suggesting that for this compound the SO_2 release is ultrafast and takes place within the excitation pulse. In accord with the hypothesis of ultrafast SO_2 release in PtPd-SO_2 **12**, comparison of the transient absorption spectra measured at 0.25 and 200 ps (Figure S8, Supporting Information) shows that already at 250 fs the transient absorption spectrum matches the difference absorption spectrum. Thus, we conclude that in clusters with mixed metal sites the photoinduced release of SO_2 is significantly faster than for the SO_2 adducts **5** and **13** of the homometal compounds Pt_2 **1** and Pd_2 **8**, most likely because of the metal−metal bonding asymmetry that is present in the mixed metal clusters, and which would reinforce the sequential asymmetric scission of the M-SO_2 bonds suggested above for the homometal compounds.

Continuous Irradiation. The reversible uptake of the studied gas molecules under UV−vis irradiation described above also may be observed on the macroscopic scale, and we also probed the reversibility of the adduct formation, as well as compound photostability, under the condition of continuous irradiation (λ > 370 nm). With Pt_2-O_2 **3**, the cycling of a sequence of irradiation periods of 20 s, alternating with dark intervals, shows that nearly 60% conversion to the dioxygen-free compound Pt_2 **1** is reached in about 10 s of irradiation (Figure 12A). The rebinding of O_2 occurs within 20 s in the dark interval. The photostability of the Pt_2 **1** compound under the irradiation conditions used is demonstrated by longer irradiation periods which lead to a constant stationary concentration, also about 60% (Figure 12B). It therefore appears that the release and rebinding of O_2 can be cycled with high efficiency without considerable photodegradation of the Pt_2 cluster. Pt_2-CO **4** behaves similarly (Figures S9, S10, Supporting Information), but, in agreement with the higher affinity of CO toward Pt_2 **1** compared to O_2, the maximum stationary concentration of photoproduced **1** is about 10%, rather than the 60% observed for Pt_2-O_2 **3**. The Pt_2-SO_2 **5** complex, in which the SO_2 molecule is the most strongly bound of the series reported here, does not show release under these

dx.doi.org/10.1021/ic200374k |*Inorg. Chem.* 2011, 50, 7511–7523

Table 2. Crystallographic Data for Pd_2 8, PtPd-CO 10, Pd_2-CO 11, PtPd-SO_2 12, and Pd_2-SO_2 13

[a]	8	10	11	12	13
formula	$C_{32}H_{54}B_{10}P_4Pd_2$	$C_{33}H_{54}B_{10}OP_4PdPt$	$C_{33}H_{54}B_{10}OP_4Pd_2 \cdot CHCl_3$	$C_{32}H_{54}B_{10}O_2P_4PtPdS \cdot CH_2Cl_2$	$C_{32}H_{54}B_{10}O_2P_4Pd_2S \cdot C_6H_6$
difractometer	Nonius KappaCCD	Brüker X8 Apex	Brüker X8 Apex	Nonius KappaCCD	Nonius KappaCCD
size	0.16 × 0.15 × 0.12	0.35 × 0.28 × 0.03	0.19 × 0.12 × 0.02	0.07 × 0.06 × 0.01	0.31 × 0.18 × 0.13
formula wt.	883.53	1000.23	1030.97	1064.76	1025.70
color, shape	orange prism	orange plate	red prism	yellow plate	red fragment
crystal sys.	monoclinic	orthorhombic	monoclinic	orthorhombic	orthorhombic
space group	$C2/c$	$Pna2_1$	$P2_1/c$	$Pna2_1$	$Pc2_1n$
a/Å	23.4332(3)	23.566(5)	12.4922(11)	23.901(5)	23.964(5)
b/Å	11.4378(2)	10.827(2)	24.4954(22)	10.743(2)	10.788(2)
c/Å	17.2521(3)	17.533(4)	15.7457(13)	17.573(4)	17.682(4)
β/deg	122.771(1)	90	97.903(4)	90	90
V/Å^3	3888.03(11)	4473.6(16)	4772.4(7)	4512.2(16)	4571.4(16)
D_{calc}/g·cm^{-3}	1.509	1.485	1.435	1.65	1.49
F_{000}	1792	1976	2080	2216	2088
data/restr/par	4457/0/221	11046/1/548	11803/0/507	9819/1/502	8929/10/498
extinction parameter				0.00114(10)	
μ mm^{-1}	1.114	3.694	1.083	3.833	1.006
GOF	1.055	1.032	1.023	1.025	1.034
$R1$ ($I > 2\sigma(I)$)	0.0323	0.0243	0.0361	0.0469	0.0433
$wR2$ (all data)	0.0761	0.0631	0.0879	0.0961	0.1038
$\rho_{max\ and\ min}$ /e$^-$ Å^{-3}	0.83 and −1.42	0.66 and −1.46	1.246 and −1.162	1.11 and −1.05	1.25 and −0.97
Flack		0.022(5)		0.026(8)	

[a] Common factors. All measured at 150(2) K, $Z = 4$.

conditions whereas PtPd-SO_2 **12**, which binds SO_2 less strongly, exhibits well-measurable changes because of the release of SO_2 (Figure S11, Supporting Information). Pd_2-SO_2 **13** also releases SO_2 under these conditions, but now the release and rebinding sequence is accompanied by significant compound photodegradation.

CONCLUSIONS

Predictive DFT work suggested that PtPd **7** and Pd_2 **8** would be synthetically viable targets, and that CO and SO_2 would bind to them in an analogous manner to that established for Pt_2 **1**. In addition, DFT calculations suggested that the Pd_2 **8** would bind SO_2 and CO more weakly than the corresponding diplatinum compound Pt_2 **1**, thus allowing for reversibility observed earlier for the uptake of SO_2 and CO addition in a similar manner to that observed previously for the reversible uptake of O_2 by Pt_2 **1**. Experiments then successfully showed that the binding of the molecules is indeed progressively weaker in the sequence {PtPt} → {PtPd} → {PdPd}. The binding of CO is shown to be weakened sufficiently that ready reversibility of CO and SO_2 uptake was observed for the Pd_2 **8** bimetallic site and to a lesser extent for the PtPd **7** compound.

We found that the sequestered molecules could be ejected by UV−vis irradiation. Very interesting consequences follow from the discovery of the light-activated control of the gas molecule release. Fast and spatiotemporal control of active molecule delivery are fundamental criteria for any potential application of these gas-releasing systems,[23] and the on/off triggering by light described here satisfies both of these requirements. Other additional important features imposed on such delivery systems are photostability, the ability to reversibly bind the active molecules, the possibility to follow the course of the binding/release processes, and the accurate prediction of system improvements; these are all addressed in this work. In this context it is noteworthy that the dioxygen adduct Pt_2-O_2 **3** releases dioxygen upon UV−vis irradiation with high quantum yields, and, moreover, a fraction of the dioxygen is released in singlet configuration.

The results show that the tailoring of this system by variation of metal is highly viable and useful, and that DFT predictions are a very useful aid to predicting viable targets and therefore optimizing the use of valuable synthetic bench time. The results augur well for future tailoring and fine-tuning of this system by variation of metal and metal ligand, by variation of boron cluster substituent, or by cluster constituents, such as replacing B by C, S, and so forth (as a fourth way of modification), and also for extension to other small molecules, not only in terms of sequestration, but also in terms of activation. In this latter regard there is potential here for these B-frame bimetallics to rival the very extensively investigated area of so-called "A-frame" bimetallics in versatility and consequent utility, and we hope to explore all these possibilities.

EXPERIMENTAL SECTION

General Procedures. All reactions were carried out under standard vacuum or inert-atmosphere techniques, although subsequent operations were generally carried out in air, except for a number of those involving solutions of the oxygen-sensitive $[(PMe_2Ph)_4PtPd\text{-}B_{10}H_{10}]$ **7** and $[(PMe_2Ph)_4Pd_2B_{10}H_{10}]$ **8**. $B_{10}H_{14}$ was obtained commercially (Katchem, Prague). Dichloromethane, hexane, and pentane (Fluka) were dried over appropriate desiccants and stored in 500 mL RB flasks fitted with Teflon vacuum taps and transferred by vacuum distillation into vessels cooled by liquid N_2. $KHBEt_3$ (Aldrich, 1.0 M THF solution) was used as received. Other starting materials were of reagent or analytical grade and were used as purchased. Reactions were generally carried out in a 5 mm o.d. NMR tube with a vacuum tight

dx.doi.org/10.1021/ic200374k |Inorg. Chem. 2011, 50, 7511–7523

Teflon screw cap. [*cis*-$PtCl_2(PMe_2Ph)_2$] was made by the literature route[24] from stirred water mixtures of $K_2[PtCl_4]$ and PMe_2Ph. $[(PMe_2Ph)_2PtB_{10}H_{12}]$ was made essentially according to the method reported earlier[25] in yields of about 90%. $[PdCl_2(PMe_2Ph)_2]$ was prepared using ethanol solutions of $K_2[PdCl_4]$ and PMe_2Ph from which the $[PdCl_2(PMe_2Ph)_2]$ precipitates. The resultant yellow suspension was filtered and washed with a small amount of alcohol to obtain the $[PdCl_2(PMe_2Ph)_2]$ and was used without further purification. $[(PMe_2Ph)_2PdB_{10}H_{12}]$ was made by addition of $[PdCl_2(PMe_2Ph)_2]$ to a stirred solution of $B_{10}H_{14}$ in CH_2Cl_2 that also contained 2 equiv of 1,8-bis-(dimethylamino)naphthalene ("Proton Sponge"), followed by flash chromatography down a silica-gel column (70/30 CH_2Cl_2/*n*-hexane). To achieve a maximum yield of $[(PMe_2Ph)_2PdB_{10}H_{12}]$ the ethanol filtrate from the preparation of $[PdCl_2(PMe_2Ph)_2]$ was reduced to dryness on a rotary evaporator, redissolved in CH_2Cl_2 and added to a CH_2Cl_2 solution containing excess $B_{10}H_{14}$ and Proton Sponge; the mixture was then stirred overnight and then also subjected to flash column chromatography. This procedure allows an almost quantitative overall yield of $[(PMe_2Ph)_2PdB_{10}H_{12}]$.

Criteria of purity consisted of clean ^{11}B, ^1H, and ^{31}P NMR spectra consistent together with molecular and crystal structures obtained by single-crystal X-ray diffraction analyses. A range of mass spectrometry techniques were attempted on all the compounds reported here but none gave identifiable fragments.

NMR spectroscopy was performed at about 5.9 and 11.75 T (fields corresponding to nominal 250 and 500 MHz ^1H frequencies respectively) using commercially available instrumentation and using techniques and procedures as adequately described and enunciated elsewhere.[26] Chemical shifts δ are given in ppm relative to Ξ = 100 MHz for $\delta(^1H)$ (±0.05 ppm) (nominally tetramethylsilane, $Si(CH_3)_4$), Ξ = 32.083972 MHz for $\delta(^{11}B)$ (±0.5 ppm) (nominally Et_2OBF_3 in $CDCl_3$) and Ξ = 40.480730 MHz for $\delta(^{31}P)$ (±0.5 ppm) (nominally 85% aqueous H_3PO_4), calibrations being effected by use of solvent deuteron or residual proton signals as internal secondary standards. Ξ is as defined by McFarlane.[27] Cluster ^{11}B and ^1H NMR data are presented as assignment $\delta(^{11}B)$ [$\delta(^1H)$ for directly bound H(exo) in brackets]. IR spectra were recorded on a Perkin-Elmer Spectrum One FT-IR spectrometer using a diamond cell or on a KBr plate in a Nicolet Nexus 670 FT-IR spectrometer.

Calculations were carried out using the Gaussian 03 package.[10a] Structures were initially optimized using standard ab initio methods with the STO-3G* basis-sets for B, C, P, S, N, and H, with the LANL2DZ basis-set for the metal atoms. The final optimizations, including frequency analyses to confirm the true minima, were performed using B3LYP methodology with 6-31G* and LANL2DZ basis-sets.[10b−e] In all cases the compounds were modeled using hydrogen atoms rather than organyl groups on the phosphine ligands to reduce computation time. Computed carbonyl frequencies were scaled with a 0.9613 scaling factor.[28]

Syntheses. *Improved Preparation of [$(PMe_2Ph)_4Pt_2B_{10}H_{10}$] ($Pt_2$* ***1****).* (Case A) Toluene (20 mL) was injected through a septum into a two-neck round-bottomed flask containing $[(PMe_2Ph)_2PtB_{10}H_{12}]$ (0.202 g, 0.341 mmol) and a stir bar. The mixture was cooled in a dry ice bath to −71 °C and $KHBEt_3$ (0.68 mL, 0.68 mmol) then injected, after which the mixture was allowed to warm slowly to −30 °C, giving a colorless solution. The temperature was lowered to −50 °C, $[PtCl_2(PMe_2Ph)_2]$ (0.155 g, 0.34 mmol) added against a flow of nitrogen, the stirring continued, and the mixture allowed to warm slowly to room temperature. A clear orange solution quickly formed which gradually darkened with a dark solid appearing on the bottom of the flask. The next day the mixture was filtered giving 0.178 g of dark purple microcrystalline solid which was quickly washed with benzene, then pentane. A further 0.096 g was scraped from the wall of the reaction vessel affording 0.274 g, 0.258 mmol, 76% of Pt_2 **1**.[1b]

(Case B) PMe_2Ph (0.2 mL, 1.4 mmol) was injected into a suspension of $[(PMe_2Ph)_2PtB_{10}H_{12}]$ (0.342 g, 0.557 mmol) in degassed toluene (100 mL), and the solution heated at reflux under nitrogen overnight. The color slowly changed from yellow to brown/dark purple. After cooling and rapid filtration in air, washing with benzene gave microcrystalline Pt_2 **1** (0.157 g, 0.148 mmol; 53% yield based on Pt).

In both cases A and B, purification of Pt_2 **1** is better done by filtration of CH_2Cl_2 solutions in air and crystallization from aerated CH_2Cl_2/hexane solution stored at < −20 °C. This procedure gives the orange-colored Pt_2-O_2 **3**, from which compound Pt_2 **1** may be easily regenerated in situ for further experimentation by purging solutions of the compound with an inert gas.

Preparation of [$(PMe_2Ph)_4PtPdB_{10}H_{10}$] (PtPd ***7****).* The above procedure for **1** was followed with $[(PMe_2Ph)_2PtB_{10}H_{12}]$ (0.099 g, 0.167 mmol) in toluene (23 mL) and $KHBEt_3$ (0.34 mL, 0.34 mmol) added. After allowing to warm to −30 °C the temperature was reduced to −50 °C and $[PdCl_2(PMe_2Ph)_2]$ (0.076 g, 0.168 mmol) added against a flow of nitrogen, and the reaction mixture allowed to warm slowly to room temperature with stirring. Subsequently, a purple-brown solid was obtained by filtration after washing with benzene and pentane. The solid was dissolved in CH_2Cl_2, passed through a sintered glass filter, crystallized from CH_2Cl_2/*n*-pentane at about −20 °C, and identified it as $[(PMe_2Ph)_4PtPdB_{10}H_{10}]$ by multielement NMR spectroscopy (51 mg, 0.052 mmol, 31%). Elem. anal. for $[(PMe_2Ph)_4PtPdB_{10}H_{10}]$. CH_2Cl_2, found(calc.): C37.57(37.49) H 5.14(5.34). Attempts to obtain single-crystals suitable for X-ray analysis from dichloromethane hexane or chloroform hexane solutions were unsuccessful. NMR data (298 K, CD_2Cl_2), $\delta(^{11}B)$ [^1H]/ppm: BH(7,11), +31.9 [+5.23]; BH-(9,3,6,4,5,12) +25.3 [+4.67, +4.51(2), +4.35(2), +3.91]; BH(8,10), −23.0 [+1.14]. $\delta(^1H)$ $PMe_2(Pt)_A$: +1.71 {$N(^{31}P-^1H)$ 9.8 Hz, $^3J(^{195}Pt-^1H)$ 24.6 Hz)}, $PMe_2(Pt)_B$: +1.62 {$N(^{31}P-^1H)$ 9.2 Hz, $^3J(^{195}Pt-^1H)$ 21.4 Hz)}, $N(^{31}P-^1H)$ ca. 10 Hz; $PMe_2(Pd)_A$: +1.47 {$N(^{31}P-^1H)$ 8.2 Hz}, +1.45, $N(^{31}P-^1H)$ 7.7 Hz}, and for PPh +7.17 to +7.41 {multiplets}. $\delta(^{31}P)$/ppm, CD_2Cl_2, −50 °C: on Pt +3.5 [$^3J(^{31}P-^{31}P)$ 10, $^1J(^{195}Pt-^{31}P)$ 2640 Hz], on Pd −21.1 [$^3J(^{31}P-^{31}P)$ 10 Hz, possible $^2J(^{195}Pt-^{31}P)$ ca. 40 Hz].

Preparation of [$(PMe_2Ph)_4Pd_2B_{10}H_{10}$] ($Pd_2$ ***8****).* The above procedure as described for Pt_2 **1** was followed using toluene (100 mL) and $[(PMe_2Ph)_2PdB_{10}H_{12}]$ (0.203 g, 0.403 mmol), with 0.81 mL, 0.81 mmol, of $KHBEt_3$ solution injected at −70 °C. The mixture was allowed to warm slowly with stirring to −50 °C and held at that temperature for 30 min during which time the mixture turned brown. $[PdCl_2(PMe_2Ph)_2]$ (0.443 g, 0.403 mmol) was added against a flow of nitrogen, and the reaction mixture left to warm slowly to room temperature with stirring overnight. Next morning the mixture was quickly filtered and washed with benzene giving 0.14 g of a purple-brown solid. A further 0.065 g of solid was scraped from the walls of the reaction vessel. Both solids were identified as $[(PMe_2Ph)_4$-$Pd_2B_{10}H_{10}]$ (compound **8**, combined yield 0.234 g, 0.23 mmol; 57%). Dark red single-crystals were obtained from saturated $CDCl_3$ solutions of the compound under anaerobic conditions stored at −20 °C. Elem. anal. C_{32} H_{54} B_{10} P_4 Pd_2, found(calc.): C 43.55(43.48), H 6.17(5.97). NMR data (298 K, $CDCl_3$): BH(9,12) +29.7 [+4.41], BH(3,6) ca. +32.6 [+4.85] and (near-coincident resonances) BH(4,5,7,11) ca. +32.6 [+5.48], and BH(8,10) −20.1 [+0.99]; with $\delta(^1H)$ for PMe_2 +1.49 and +1.72 {both with $N(^{31}P-^1H)$ ca. 8 Hz}, and for PPh +7.22, +7.34 and +7.40 4H {multiplets}; also $\delta(^{31}P)$ −15.3 ppm.

Reaction of Pd_2 ***8*** *with CO to Give Pd_2-CO* ***11****.* CD_2Cl_2 (ca. 0.5 mL) was condensed into an NMR tube containing a sample of Pd_2 **8** (ca. 3 mg); the tube was then sealed, removed from the Schlenk line, and shaken to dissolve the sample. The tube was reattached to the Schlenk line and opened to an atmosphere of pure CO. A pale tan color was observed to diffuse down slowly from the top of the dark purple-red solution. Agitation of the tube eventually resulted in the disappearance of the purple-red color to form a tan-colored solution, and ^{11}B, ^{31}P, and ^1H-{^{11}B} NMR spectroscopy then indicated a complete conversion to Pd_2-CO **11**. Removal of the solvent from CH_2Cl_2 solutions of the

compound on a rotary film evaporator (water bath, ca. 30 °C) resulted in regeneration of Pd_2 **8**, pure by NMR spectroscopy. Crystals suitable for single-crystal X-ray work were obtained by diffusion of *n*-pentane through a layer of benzene into a $CHCl_3$ solution of the compound. Because of the easy loss of CO from the compound, the sample was agitated slightly to accelerate mixing and to initiate crystallization, but this caused the formation only of small crystals, which necessitated the use of a rotating-anode X-ray source to obtain a suitable data set for the diffraction analysis. Infrared, diamond cell: ν(BH) 2511br, ν(CO) 1882 cm^{-1}. NMR data (298 K, $CDCl_3$): BH(9,12) ca. +28.5 [+4.64] and (coincident boron resonances) BH(3,6) ca. +28.5 [+2.16]}, BH-(4,5,7,11) +19.6 [+4.33] and BH(8,10) −11.3 [+1.98]; with δ (^{1}H) for PMe_2 +1.26 and +1.53 {both with $N(^{31}P-^1H)$ ca. 10 Hz}, and for PPh +7.05 to +7.40 {multiplets}]; also $\delta(^{31}P)$ −14.1 ppm.

Reaction of Pd_2 ***8*** *with SO_2 to Give Pd_2-SO_2* ***13***. The procedure followed that described above for Pd_2-CO **11**. A golden coloration, rather than the tan of the CO reaction, diffused down the column of solution in the tube. Quantitative conversion was confirmed by NMR spectroscopy. Crystals suitable for single-crystal X-ray diffraction analysis were obtained by diffusion of *n*-pentane through a thin layer of benzene into a CH_2Cl_2 solution of the compound. NMR data (298 K, CD_2Cl_2): BH(9,12) +31.4 [+4.58], BH(3,6) +34.7 [+2.65], BH-(4,5,7,11) +21.3 [+4.23] and BH(8,10) −6.2 [+2.09]; with δ(^{1}H) for PMe_2 +1.25 and +1.44 {both with $N(^{31}P-^1H)$ ca. 10 Hz}, and for PPh +7.25 to +7.50 {multiplets}; also $\delta(^{31}P)$ −8.35 ppm.

Reaction of PtPd ***7*** *with CO to Give PtPd-CO* ***10***. The procedure carried out for compound **11** was repeated. Very dark red crystals suitable for single-crystal X-ray diffraction analysis were obtained by diffusion of *n*-pentane into CH_2Cl_2 solutions of the compound. NMR data (298 K, CD_2Cl_2): BH(9) ca. +23.9 [+5.29], BH(12) ca. +20.7 [+4.18]; BH(3,6) +16.6 [+1.35], BH(4,5) +14.6 [+4.08], BH(7,11) +7.3 [+3.80 {$J(^{195}Pt-^1H)$ ca. 55 Hz}] and BH(8,10) −13.9 [+2.09]; with δ(^{1}H) for $PMe_2(Pt)_A$ +1.47 {$N(^{31}P-^1H)$ 10.0 Hz, $^3J(^{195}Pt-^1H)$ 17.5 Hz)}, $PMe_2(Pt)_B$ +1.41 {$N(^{31}P-^1H)$ 10.4 Hz, $^3J(^{195}Pt-^1H)$ 22.5 Hz}, $PMe_2(Pd)_A$ +1.35 {$N(^{31}P-^1H)$ 9.6 Hz}, $PMe_2(Pd)_B$, +1.28 {$N(^{31}P-^1H)$ 9.8 Hz} and for PPh +7.28 to +7.47 {multiplets}; also $\delta(^{31}P)$ −24.6 [$^1J(^{195}Pt-^{31}P)$ 2644 Hz] and −18.1 [$^3J(^{195}Pt-^{31}P)$ 63 Hz]. Infrared, evaporated CH_2Cl_2 solution on to a KBr plate: ν(BH) 2511br, ν(CO) 1847 cm^{-1}.

Reaction of PtPd ***7*** *with SO_2 to Give PtPd-SO_2* ***12***. The addition of SO_2 induced a ginger coloration. Green-yellow microcrystals were obtained from *n*-pentane/CH_2Cl_2 solution, and yellow-plate single-crystals for X-ray diffraction analysis were obtained by diffusion of *n*-pentane into a CH_2Cl_2 solution of the compound. Anal. [$(PMe_2Ph)_4(SO_2)PtPdB_{10}H_{10}$].$CH_2Cl_2$, found(calc.): C 35.61(35.35), H 5.07-(5.03). NMR data (298 K, $CDCl_3$): BH(12) ca. +27.4 [+5.76 {antipodal coupling $^4J(^{195}Pt-^1H)$ ca. 30 Hz}(see text in Supporting Information, page S2)], BH(9) ca. +27.4 [+4.73]; BH(3,6) +24.3 [+2.15], BH(4,5) +18.0 [+4.36], BH(7,11) +9.8 [+4.08] and BH(8,10) −7.6 [+2.96 {$J(^{195}Pt-^1H)$ ca. 55 Hz}]; with δ(^{1}H) for $PMe_2(Pt)_A$ +1.49 {$N(^{31}P-^1H)$ 10.0 Hz, $^3J(^{195}Pt-^1H)$ 17.5 Hz)}, $PMe_2(Pt)_B$ +1.72 {$N(^{31}P-^1H)$ 10.4 Hz, $^3J(^{195}Pt-^1H)$ 22.5 Hz}, $PMe_2(Pd)_A$ +1.37 {$N(^{31}P-^1H)$ 9.6 Hz}, $PMe_2(Pd)_B$, +1.57 {$N(^{31}P-^1H)$ 9.8 Hz} and for PPh +7.30 to +7.55 {multiplets}; also $\delta(^{31}P)$ −10.7 [$^1J(^{195}Pt-^{31}P)$ 2605 Hz] and −13.3 [no $^3J(^{195}Pt-^{31}P)$ resolved]. [$^1H-^1H$]-COSY interactions between ^{1}H(4,5) at +4.36 and ^{1}H-(PMe_2)(Pd) at +1.37 and +1.57, and similarly between ^{1}H(7,11) at +4.08 and ^{1}H(PMe_2)(Pt) at +1.49 and +1.72, were observed, implying small but finite longer-range couplings $^5J(^1H-B-Pd-P-C-^1H)$-(*cisoid*) and $^5J(^1H-B-Pt-P-C-^1H)$(*cisoid*), but no correspondingly observable *transoid* interactions. Additionally, in ^{1}H-{^{11}B} spectra, fine doublet splittings on ^{1}H(4,5) and ^{1}H(7,11) of about 10 Hz were observable. These were more apparent in the [$^1H-^1H$]-COSY-{^{11}B} plots, which also showed a doublet splitting on ^{1}H(8,10) of about 3 Hz. The [$^1H-^1H$] correlation behavior of the individual doublet components suggest that this fine structure probably arises from phosphorus-to-proton couplings.

Single-Crystal X-ray Diffraction Analyses. Diffraction data were collected either on a Nonius KappaCCD diffractometer with a conventional sealed-tube X-ray source (λ = 0.71073 Å), or, for very small crystals, on a Brüker X8 Kappa APEX II CCD area-detector diffractometer with an FR591 rotating anode generator. In each case crystals were cooled with a dinitrogen gas stream. Absorption corrections were made by semiempirical methods. The structures were solved by automatic direct methods and refined by least-squares methods on all measured F^2 values, with a weighting scheme $w^{-1} = \sigma^2(F_o^2) + (aP)^2 + (bP)$, where $P = (F_o^2 + 2F_c^2)/3$. Residuals were defined by $R_1 = \Sigma||F_o| - |F_c||/\Sigma|F_o|$, $wR_2 = \sqrt{[\Sigma w(F_o^2 - F_c^2)^2/\Sigma w(F_o^2)^2]}$. Methods and programs were standard.[29] Crystallographic data are summarized in Table 2. The programs X-Seed[30] and Ortep-3 were[31] used as an interface to the SHELX programs, and to prepare the figures. Compounds [$(PMe_2Ph)_4$-(CO)$PtPdB_{10}H_{10}$], PtPd-CO **10**, showed a disorder involving the positions of the platinum and palladium atoms. A model of the disorder was established assuming exchange in their positions and was refined with a free variable. Further disorder involved two positions for one phosphine group plus a slight twist in one phenyl group on a second phosphine and these were also refined with a common occupancy and refined with a free variable. Disordered dichloromethane molecules were also apparent and were incorporated in the model using Platon/Squeeze.[32] [$(PMe_2Ph)_4(SO_2)PtPdB_{10}H_{10}$] **12** also showed a similar disorder but only involving an exchange in the positions of the platinum and palladium atoms.

Photophysical and Photochemical Methods. *Nanosecond Transient Absorption.* Laser flash photolysis experiments were performed with a Lambda Physik COMPEX 102 excimer (308 nm, pulse width 28 ns, incident energy up to 15 mJ/pulse) or a Lambda Physik FL 3002 dye laser (425 nm, incident energy ~1 mJ/pulse). Transient absorption spectra were measured within 450−600 nm on a laser kinetic spectrometer (Applied Photophysics, U.K.). The time profiles were recorded using a 250 W Xe lamp equipped with a pulse unit and a R928 photomultiplier (Hamamatsu). The quantum yields for the gas release were determined by the comparative technique using benzophenone as a standard (λ_{ex} = 308 nm, Φ_T = 1.0, $\Delta\varepsilon$ = 7220 M^{-1} cm^{-1} at 530 nm.[33]

Time-Resolved Luminescence of Singlet Oxygen. The near-infrared luminescence of $O_2(^1\Delta_g)$ at 1270 nm was monitored using a Ge detector (1270 nm interference filter, Judson Ge diode) upon laser excitation by a Lambda Physik COMPEX 102 excimer (λ_{exc} = 308 nm, fwhm 28 ns, incident energy up to 200 mJ/pulse). Emitted luminescence was detected at the right angle to excitation light. The signal from the detector was collected in a 600 MHz oscilloscope (Agilent Infiniium) and transferred to a computer for further analysis. The signal-to-noise ratio of the signals was improved by the averaging of 100 to 500 individual traces. The short-lived signal produced by the scattering of an excitation laser pulse was eliminated by exciting the argon-saturated sample and by subtracting the obtained signal from the signal recorded in oxygen-saturated solution. The quantum yield of singlet oxygen formation, Φ_Δ, was estimated by the comparative method using 5,10,15,20-tetrakis(pentafluorophenyl)porphyrin as a standard (Φ_Δ = 0.8).[16]

Femtosecond Transient Absorption. Femtosecond pulses were obtained from a 1 kHz femtosecond laser system (Integra-I, Quantronix). The output pulses had ~130 fs width, an average energy of ~2 mJ/pulse, and a central wavelength of 790 nm. The pulses were divided into two paths serving as excitation and probe pulses. Excitation pulses centered at 395 nm were generated by frequency doubling the primary output in a BBO crystal, while a white-light continuum obtained by focusing a fraction of the 790-nm pulses into a 0.2 cm sapphire plate was used for probing. For signal detection, the probe beam and an identical reference

beam were focused onto the entrance slit of a spectrograph, which then dispersed both beams onto a dual photodiode array detection system (ExciPro, CDP Systems). A 1-mm path length rotating quartz cell spinning at a rate ensuring that each excitation pulse hits a fresh sample was used for measurements. The mutual orientation of the excitation and probe beams was set to the magic angle (54.7°).

Continuous Irradiation. The sample dissolved in CH_2Cl_2 was placed in a sealed 1 cm sample quartz cell. The measurements were performed in a laser kinetic spectrometer LKS 20 (Applied Photophysics, U.K.) where the samples were continuously irradiated by a 250 W Xe lamp. A glass optical filter between the lamp and the irradiated cell was used to cut off the short wavelength components (λ < 370 nm) to prevent photodegradation of sample by UV light (this alignment is "light ON"). The transmitted light passed through a monochromator and was detected by an R928 photomultiplier (Hamamatsu). Irradiation was switched off by the addition of a 500 nm long pass filter between the lamp and the sample cell (this alignment is "light OFF"). In both cases transmitted light >500 nm served to probe the photochemical release of gases at the band maxima of the boron cluster adduct. The cycles light ON/light OFF were periodically repeated.

■ ASSOCIATED CONTENT

Supporting Information. Additional information includes details of the DFT calculations mentioned in the text and a listing of DFT calculated atomic coordinates, a detailed analysis of the ^{11}B NMR spectra, Figures S1 to S11, and tables of interatomic distances and angles for compounds **8** to **13** obtained from single-crystal X-ray diffraction data. This material is available free of charge via the Internet at http://pubs.acs.org.

■ AUTHOR INFORMATION

Corresponding Author

*E-mails: jbould@gmail.com (J.B.), lang@iic.cas.cz (K.L.).

■ ACKNOWLEDGMENT

This work was supported by the Czech Science Foundation (Nos. P207/11/1577, P208/10/1678), the Grant Agency of the Academy of Sciences of the Czech Republic (KAN400480701), and the Spanish Ministry of Science Innovation (projects CSD2009-50, CTQ2009-10132, and a sabbatical leave, SAB2009-0191, to J.B.). We thank Simon Barrett for assistance with NMR spectroscopy and Colin Kilner for crystallographic data collection. Aspects of the work have been supported by personal financial contributions from J.B. The authors would like to thank to Pavel Chábera and Václav Šlouf (University of South Bohemia, Nové Hrady) for technical help with femtosecond experiments.

■ REFERENCES

(1) (a) Bould, J.; McInnes, Y. M.; Carr, M. J.; Kennedy, J. D. *Chem. Commun.* **2004**, 2380. (b) Bould, J.; Kilner, C. A.; Kennedy, J. D. *Dalton Trans.* **2005**, 1574.

(2) (a) Maneiro, M.; Fernandez, B.; Gomez-Forneas, E.; Rodriguez, M. J.; Pedrido, R.; Romero, M. J.; Bermejo, M. R. *Z. Anorg. Allg. Chem.* **2005**, *631*, 2000. (b) Vaska, L.; Bath, S. S. *J. Am. Chem. Soc.* **1966**, *88*, 1333.

(3) (a) Benner, L. S.; Olmstead, M. M.; Hope, H.; Balch, A. L. *J. Organomet. Chem.* **1978**, *153*, C31. (b) Albrecht, M.; Gossage, R. A.; Lutz, M.; Spek, A. L.; van Koten, G. *Chem.—Eur. J.* **2000**, *6*, 1431.

(4) Pringle, P. G.; Shaw, B. L. *J. Chem. Soc., Dalton Trans.* **1983**, 889.

(5) Balch, A. L.; Benner, L. S.; Olmstead, M. M. *Inorg. Chem.* **1979**, *18*, 2996.

(6) (a) Olmstead, M. M.; Hope, H.; Benner, L. S.; Balch, A. L. *J. Am. Chem. Soc.* **1977**, *99*, 5502. (b) Bhaduri, S.; Casella, L.; Ugo, R.; Raithby, P. R.; Zuccaro, C.; Hursthouse, M. B. *J. Chem. Soc., Dalton Trans.* **1979**, 1624.

(7) Tyeklar, Z.; Jacobson, R. R.; Wei, N.; Murthy, N. N.; Zubieta, J.; Karlin, K. D. *J. Am. Chem. Soc.* **1993**, *115*, 2677.

(8) Vaartstra, B. A.; Xiao, J. L.; Cowie, M. *J. Am. Chem. Soc.* **1990**, *112*, 9425.

(9) Cheek, Y. M.; Kennedy, J. D.; Thornton-Pett, M. *Inorg. Chim. Acta* **1985**, *99*, L43.

(10) (a) Frisch, M. J.; Trucks, G. W.; Schlegel, H. B.; Scuseria, G. E.; Robb, M. A.; ; Cheeseman, J. R.; Jr., J. A. M.; Vreven, T.; Kudin, K. N.; Burant, J. C.; J. M.Millam; Iyengar, S. S.; Tomasi, J.; Barone, V.; Mennucci, B.; ; Cossi, M.; Scalmani, G.; Rega, N.; Petersson, G. A.; Nakatsuji, H.; Hada, M.; Ehara, M.; Toyota, K.; Fukuda, R.; Hasegawa, J.; Ishida, M.; Nakajima, T.; Honda, Y.; Kitao, O.; Nakai, H.; Klene, M.; Li, X.; Knox, J. E.; Hratchian, H. P.; Cross, J. B.; Bakken, V.; Adamo, C.; Jaramillo, J.; ; Gomperts, R.; Stratmann, R. E.; Yazyev, O.; Austin, A. J.; Cammi, R.; ; Pomelli, C.; Ochterski, J.; Ayala, P. Y.; Morokuma, K.; Voth, G. A.; Salvador, P.; Dannenberg, J. J.; Zakrzewski, V. G.; Dapprich, S.; Daniels, A. D.; Strain, M. C.; Farkas, O.; Malick, D. K.; Rabuck, A. D.; Raghavachari, K.; Foresman, J. B.; Ortiz, J. V.; Cui, Q.; Baboul, A. G.; Clifford, S.; Cioslowski, J.; Stefanov, B. B.; Liu, G.; Liashenko, A.; Piskorz, P.; ; Komaromi, I.; L.Martin, R.; Fox, D. J.; Keith, T.; Al-Laham, M. A.; Peng, C. Y.; Nanayakkara, A.; Challacombe, M.; Gill, P. M. W.; Johnson, B. G.; Chen, W.; Wong, M. W.; Gonzalez, C.; Pople, J. A. *GAUSSIAN 03*, Rev. C.02; Gaussian, Inc: Wallingford, CT, 2004. (b) Becke, A. D. *J. Chem. Phys.* **1993**, *98*, 5648. (c) Lee, C.; Yang, W.; Parr, R. G. *Phys. Rev. B* **1988**, *37*, 785. (d) Hehre, W. J.; Ditchfield, R.; Pople, J. A. *J. Chem. Phys.* **1972**, *56*, 2257. (e) Hay, P. J.; Wadt, W. R. *J. Chem. Phys.* **1985**, *82*, 299.

(11) Le Guennic, B.; Jiao, H.; Kahlal, S.; Saillard, J. Y.; Halet, J. F.; Ghosh, S.; Shang, M.; Beatty, A. M.; Rheingold, A. L.; Fehlner, T. P. *J. Am. Chem. Soc.* **2004**, *126*, 3203.

(12) Bould, J.; Kennedy, J. D. *Chem. Commun.* **2008**, 2447.

(13) Mikšovská, J.; Norstrom, J.; Larsen, R. W. *Inorg. Chem.* **2005**, *44*, 1006.

(14) Zhou, X.; Pan, Q.-H.; Li, M.-X.; Xia, B.-H.; Zhang, H.-X. *J. Mol. Struct.* **2007**, *822*, 65.

(15) Lang, K.; Mosinger, J.; Wagnerová, D. M. *Coord. Chem. Rev.* **2004**, *248*, 321.

(16) Cavaleiro, J. A. S.; Görner, H.; Lacerda, P. S. S.; MacDonald, J. G.; Mark, G.; Neves, M. G. P. M. S.; Nohr, R. S.; Schuchmann, H.-P.; von Sonntag, C.; Tomé, A. C. J. *Photochem. Photobiol. A* **2001**, *144*, 131.

(17) (a) Valentine, D.; Valentine, J. S. *Inorg. Chem.* **1971**, *10*, 393. (b) Vogler, A.; Kunkely, H. *Coord. Chem. Rev.* **2006**, *250*, 1622.

(18) Seip, M.; Brauer, H.-D. *J. Photochem. Photobiol. A.* **1994**, *79*, 19.

(19) Seip, M.; Brauer, H.-D. *J. Photochem. Photobiol. A.* **1993**, *76*, 1.

(20) Vogler, A.; Kunkely, H. *J. Am. Chem. Soc.* **1981**, *103*, 6222.

(21) Rupenyan, A.; Commandeur, J.; Groot, M. L. *Biochemistry* **2009**, *48*, 6104.

(22) Kapetanaki, S. M.; Field, S. J.; Hughes, R. J. L.; Watmough, N. J.; Liebl, U.; Vos, M. H. *Biochim. Biophys. Acta, Bioenerg.* **2008**, *1777*, 919.

(23) (a) Sortino, S. *Chem. Soc. Rev.* **2010**, *39*, 2903. (b) Crespy, D.; Landfester, K.; Schubert, U. S.; Schiller, A. *Chem. Commun.* **2010**, *46*, 6651. (c) Alberto, R.; Motterlini, R. *Dalton Trans.* **2007**, 1651.

(24) Parshall, G. W. *Inorg. Synth.* **1970**, *12*, 27.

(25) Wrackmeyer, B.; Kennedy, J. D. *J. Magn. Reson.* **1980**, *38*, 529.

(26) (a) Kennedy, J. D. *Multinuclear NMR*; Mason, J., Ed.; Plenum: New York and London, 1987; p 221. (b) Reed, D. *Chem. Soc. Rev.* **1993**, *22*, 109. (c) Heřmánek, S. *Chem. Rev.* **1992**, *92*, 325. (d) Ferguson, G.; Kennedy, J. D.; Fontaine, X. L. R.; Faridoon; Spalding, T. R. *J. Chem. Soc., Dalton Trans.* **1988**, 2555.

(27) McFarlane, W. *Proc. R. Soc. (London), Series A* **1968**, *306*, 185.

(28) Merrick, J. P.; Moran, D.; Radom, L. J. *Phys. Chem. A* **2007**, *111*, 11683.

(29) (a) *COLLECT: Data Collection Strategy Program*; Nonius: Delft, The Netherlands, 1999. (b) Otwinowski, Z.; Minor, W. *Methods*

Enzymol. **1997**, *276*, 307. (c) *SHELXTL manual*; Bruker AXS: Madison, WI, 1994 and 1998. (d) Sheldrick, G. *Acta Crystallogr., Sect. A.* **2008**, *64*, 112.
(30) Barbour, L. J. *J. Supramol. Chem.* **2001**, *1*, 189.
(31) Farrugia, L. J. *J. Appl. Crystallogr.* **1997**, *30*, 565.
(32) Sluis, P. v. d.; Spek, C. A. *Acta Crystallogr., Sect. A.* **1990**, *46*, 194.
(33) Hurley, J. K.; Sinai, N.; Linschitz, H. *Photochem. Photobiol.* **1983**, *38*, 9.